Computer Assisted Methods in Engineering and Science
32(3): 237–253, 2025, https://doi.org/10.24423/cames.2025.1869

Parametric Analysis of Damage in Cancellous Bone and in Materials with Bone-like Microstructure

Piotr KOWALCZYK

Institute of Fundamental Technological Research, Polish Academy of Sciences, Warsaw, Poland; e-mail: piotr.kowalczyk@ippt.pan.pl

A systematic approach to the macroscopic damage analysis of bone-like cellular materials is presented in which damage conditions are expressed as tabularized functions of microstructure geometry parameters. Based on three different strain-based microscopic damage criteria, a large number of cellular microstructures, characterized by different values of geometric parameters, are analysed by the finite element method to determine damage factor values for a number of macroscopic strain states. As a result, an exhaustive database is prepared in which macroscopic damage conditions for a variety of microstructures are presented as tabularized parametric functions of both geometric parameters and strain states. A numerical procedure of data interpolation is proposed as a tool to predict parameterized damage surfaces for any bone-like microstructure. The results are made publicly available in an open data repository to enable further research on their characterization and analytical approximation.

Keywords: cancellous bone, damage properties, parametric studies, finite element (FE) analysis.

1. Introduction

A challenging branch of biomechanical research regarding bone is the analysis of its damage. In particular, this refers to damage properties of cancellous bone – a porous bone microstructure made up of trabeculae. This subject has attracted much attention of researchers over at least the past three decades. Both experimental and numerical methods have been utilized to predict bone damage conditions at a number of scales: micro (tissue level), meso (trabecular level) and macro (whole bone level). The two main challenges in this research area are: (i) determination of the damage criterion for trabecular bone tissue, and (ii) formulation of the macroscopic damage criterion for cancellous bone considered as macroscopic continuum.

The fundamental obstacle regarding the first issue is the lack of experimental data which is due to the fact that reliable strength tests are extremely difficult

to be performed on objects of such small size. Only few experiments have been reported in literature, e.g., [4] (tensile tests only). On the other hand, successful attempts have been reported to predict micro-level properties by comparing macroscopic experimental measurements against the results of numerical simulations of experiments on models that reproduce the trabecular geometry of the specimens. This approach was originally developed to evaluate bone elastic properties [16], but has since been successfully utilized in predicting damage properties at the microscopic level, see e.g. [13] (for bovine), and [2] (for human bone). Mechanical experiments are performed on cancellous bone specimens to measure macroscopic (apparent) damage stresses/strains and then micro-FE analyses are performed on the CT-scanned geometric models of these specimens in which load and boundary conditions reproduce those from the experiments. By presuming certain (strain or stress-based) local damage criteria, one can determine the damage limit values at which the macroscopic damage in the analysed model best fits the experimentally measured damage.

There is a common agreement about the hypothesis that damage in cortical bone is strain-driven [12] and that the mechanical properties of cortical bone tissue can be extrapolated to describe trabecular tissue as well [2]. Besides, it is commonly assumed that trabecular tissue is isotropic (in fact, it is not, but there is evidence that neglecting anisotropy does not significantly affect the results of macroscopic analysis of cancellous structures [6]). Thus, microscopic damage criteria for trabecular tissue are usually formulated in terms of strain invariants, i.e., limit values of certain strain-defined scalar quantities (damage factors) are proposed as damage criteria. Among a number of damage factors proposed in the literature, one can list, e.g., maximum principal strain (separately for tension and compression) [2, 5, 13] or dimensionless strain energy [14]. It is noteworthy that stress-defined damage factors, which are also proposed in the literature, such as Huber–von Mises stress [7,8], may as well be expressed in terms of strain invariants – in isotropic elastic material models this only requires appropriate scaling by elastic constants. Several other damage factors were also mentioned and discussed in the literature, such as, e.g., maximum shear strain or stress-defined quantities according to the Tresca, Coulomb–Mohr or Hoffman theories. However, they were reported to be less appropriate to modelling bone damage than the strain-defined ones mentioned above [7].

Given a local damage criterion and the geometry of the trabecular microstructure, one can easily predict the overall strength of cancellous bone at the macro scale using numerical analysis employing, e.g., the finite element (FE) method. Many examples of such analyses have been reported, both for isolated cancellous bone specimens and for entire bones, let us mention, e.g., [1,5,13–15]. By digitizing a typical cancellous bone specimen and subjecting its FE model to a number of prescribed load cases that correspond to certain averaged macro-

scopic stress/strain states, one can examine local strain conditions in view of the prescribed damage criterion and define points in the strain component space that correspond to the damage limit for the macroscopic strain states under consideration. When the set of analysed macroscopic strains is sufficiently large and diverse, the results form a cloud of points that define the macroscopic damage limit surface in the strain component space.

A disadvantage of this approach is that the results are valid only for the very specimen analysed, characterized by the particular trabecular microstructure, and cannot be generalized towards other microstructure types whose variety seems unlimited. The question of defining a universal approach to determine damage surfaces for various cancellous bone types remains open.

In this paper, a step towards resolving this problem is made. A concept of a parametrized family of bone-like microstructures was proposed in [9] and then enhanced in [10]. The mechanical properties of these microstructures have been proven to correspond well to real cancellous bone properties, see discussion in [3, 10]. Besides, it was shown in [10] that the geometric parameters defining different instances of equivalent trabecular microstructures are indirectly related to standard morphometric parameters, which can be measured in the micro-CT scans of real cancellous bones.

These equivalent bone microstructures have now been analysed by FE techniques for a number of assumed local damage criteria. As a result, a large data base of tabularized strain functions has been created, which allows to predict macroscopic damage limit strain states for a predefined set of microscopic geometric parameter values. This data base, made publicly accessible, constitutes an exhaustive source to formulate parameterized damage surfaces for different cancellous bone types.

2. Methods

2.1. Microstructure geometry

The family of parameterized trabecular microstructures [10] is defined by a repeatable cell presented in Fig. 1. It is parameterized by three geometric parameters: t_c, t_h, $t_v \in (0, 1)$, defining the cross-section proportions of trabeculae.[1)] These parameters are dimensionless and intended to be scaled by the prescribed cell unit size. The latter can be adjusted to match the actual trabecular spacing; however, as the homogenization results appear to be size-independent,

[1)] In the original publication, a fourth parameter was also introduced – a scale factor for the entire cell in the x_1 direction – to introduce more diversity in the material's orthotropy. Here we limit ourselves to setting this factor equal to 1 which corresponds to transversal isotropy of the macroscopic cellular material.

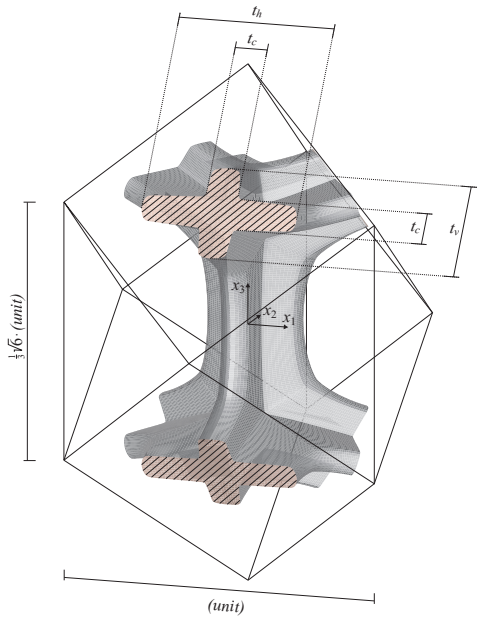

FIG. 1. Geometry of a repeatable structural cell [10]. Striped areas denote the common interfaces with neighboring cells. The cell size is assumed a unitary value, to be scaled by the actual average trabecular spacing.

this issue is not crucial. Clustered cells fill the 3D space and form a cellular material mimicking cancellous bone of the given microstructure type. As shown in [10], various combinations of these parameter values result in a variety of microstructure types, such as bar network, parallel plates with spacer bars, honeycomb tube or cluster of fenestrated boxes. Figure 2 presents an example of a microstructure generated by the repeatable cell.

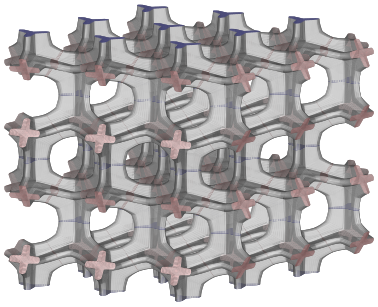

FIG. 2. Example of a microstructure generated by the repeatable cell with geometric parameters $t_c = 0.1$, $t_h = t_v = 0.4$.

Given the local (microscopic) material properties of the trabecular tissue and the values of the geometric parameters, one can build a FE model of the

repeatable cell and – for appropriate load and boundary conditions – perform an analysis whose result is a set of desired macroscopic mechanical properties of the resultant cellular material. This approach was successfully employed in [10], where an extensive database of the elastic properties of such equivalent microstructures was created for a large number of geometric parameters' values sets. This database constitutes the basis to formulate the parametric functions of the elastic properties with respect to the microstructure geometric parameters.

In this paper, this approach is applied to evaluate the damage properties of the parameterized family of microstructures. A set of 2470 microstructure instances, characterized by t_c, t_h, t_v independently running over the set of values: 0.05, 0.10, 0.15, ..., 0.95 (for obvious reasons $t_h \geq t_c$ and $t_v \geq t_c$) were meshed and subjected to an FE analysis whose details are described further below. It must be noted that only some of these instances correspond to real trabecular microstructures (mainly those with low values of t_c); however, all were analysed to make the results complete, also bearing in mind possible non-biomechanical applications of these results.

2.2. Analysis methods

The cell geometry and FE meshes were generated by the author's custom software while all analyses were performed with Simulia® ABAQUS® Standard code. In each analysis, loads were imposed by prescribing displacements at the central points of common interfaces (the striped areas in Fig. 1) and assuming appropriate boundary conditions ensuring the repeatability of the displacement field in neighboring cells (including appropriate symmetries), see [10] for details. The prescribed displacements define a unique macroscopic averaged strain state in the cell.

Each microstructure instance was subjected to a number of different loads corresponding to macroscopic (averaged over the cell volume) strain states, given by:

$$[E_{11},\, E_{22},\, E_{33},\, E_{23},\, E_{31},\, E_{12}] = 0.001 \times [a_1,\, a_2,\, a_3,\, a_4,\, a_5,\, a_6], \tag{1}$$

where a_k, $k = 1, ..., 6$, independently run over the set of values: $\{-1,\, -0.5,\, 0,\, 0.5,\, 1\}$, i.e., they form a 5^6 regular mesh of points within a double-unit hypercube in the 6D space of strain components. To avoid redundancy of results, the strain cases corresponding to points located inside the hypercube were excluded from this set, i.e., the analysed load cases included only "surface" strain states in which at least one strain component equals ± 0.001. The total number of all load cases analysed was thus $5^6 - 3^6 = 14\,896$ for each microstructure instance.

In this work, the damage is understood as the loss of material integrity manifested by a sudden drop in stiffness and the appearance of inelastic phenomena.

In the analysis, we stopped at this moment and did not attempt to investigate what happens further, when the local strains increase beyond the damage limit (which may ultimately lead to fracture). Hence, all FE analyses were limited to the linear elastic regime. Since only strains, not stresses, were evaluated in the analysis, the Young modulus E of the trabecular tissue was not a crucial quantity and was simply assumed to be one. The Poisson ratio of the material was set to the commonly accepted value $\nu = 0.3$. Strains at the Gauss integration points in all the finite elements of the model were reported as results and were examined against a number of assumed damage criteria.

2.3. Local damage criteria

The local (microscopic) damage criteria considered in this work for the trabecular tissue have the common form

$$\overline{\varepsilon} \leq \epsilon_d, \tag{2}$$

where $\overline{\varepsilon}$ is a damage factor specific to the particular criterion, expressed as a function of strain components ε_{ij}, and ϵ_d is the damage limit value. All strain states at which $\overline{\varepsilon} = \epsilon_d$ form a hyper-surface in the 6D space of strain components, further called the damage surface, which limits the domain of safe (undamaged) states. Varying the limit value of ϵ_d scales the surface without changing its shape.

Among a number of damage factors proposed in the literature, the following are considered in this work:

- Maximum principal strain [2, 5, 13]

$$\overline{\varepsilon} = \overline{\varepsilon}^{\,\mathrm{Pt}} = \varepsilon_{\mathrm{I}} \quad \text{(tension)}, \qquad \overline{\varepsilon} = \overline{\varepsilon}^{\,\mathrm{Pc}} = -\varepsilon_{\mathrm{III}} \quad \text{(compression)}, \tag{3}$$

  (with two different damage limits, ϵ_d^{t} and ϵ_d^{c}, respectively),

- Energy-based effective strain [14]

$$\overline{\varepsilon} = \overline{\varepsilon}^{\,\mathrm{U}} = \sqrt{2U/E} = \sqrt{\frac{1}{2(1+\nu)}\left(\varepsilon_{ij}\varepsilon_{ij} + \frac{\nu\,\varepsilon_{ii}\varepsilon_{jj}}{1-2\nu}\right)}, \tag{4}$$

- Huber–von Mises strain (scaled Huber–von Mises stress) [7, 8]

$$\overline{\varepsilon} = \overline{\varepsilon}^{\,\mathrm{HM}} = \frac{\overline{\sigma}^{\,\mathrm{HM}}}{G} = \sqrt{\frac{3}{2}\varepsilon_{ij}^{\mathrm{D}}\varepsilon_{ij}^{\mathrm{D}}}, \tag{5}$$

where $\varepsilon_{\mathrm{I}} \geq \varepsilon_{\mathrm{II}} \geq \varepsilon_{\mathrm{III}}$ are the principal strains, $\varepsilon_{ij}^{\mathrm{D}}$ represents the deviatoric strain components, and E, G, ν are the tissue's elastic constants. In the case of the first, double criterion, the damage surface consists of two patches – parts of two surfaces that limit the domain of safe states with respect to both criteria.

In Fig. 3, the damage surfaces corresponding to the three above-mentioned damage criteria are depicted in three 3D subspaces of the 6D strain components space. Their shapes are regular, and they can all be described by quadric equations.

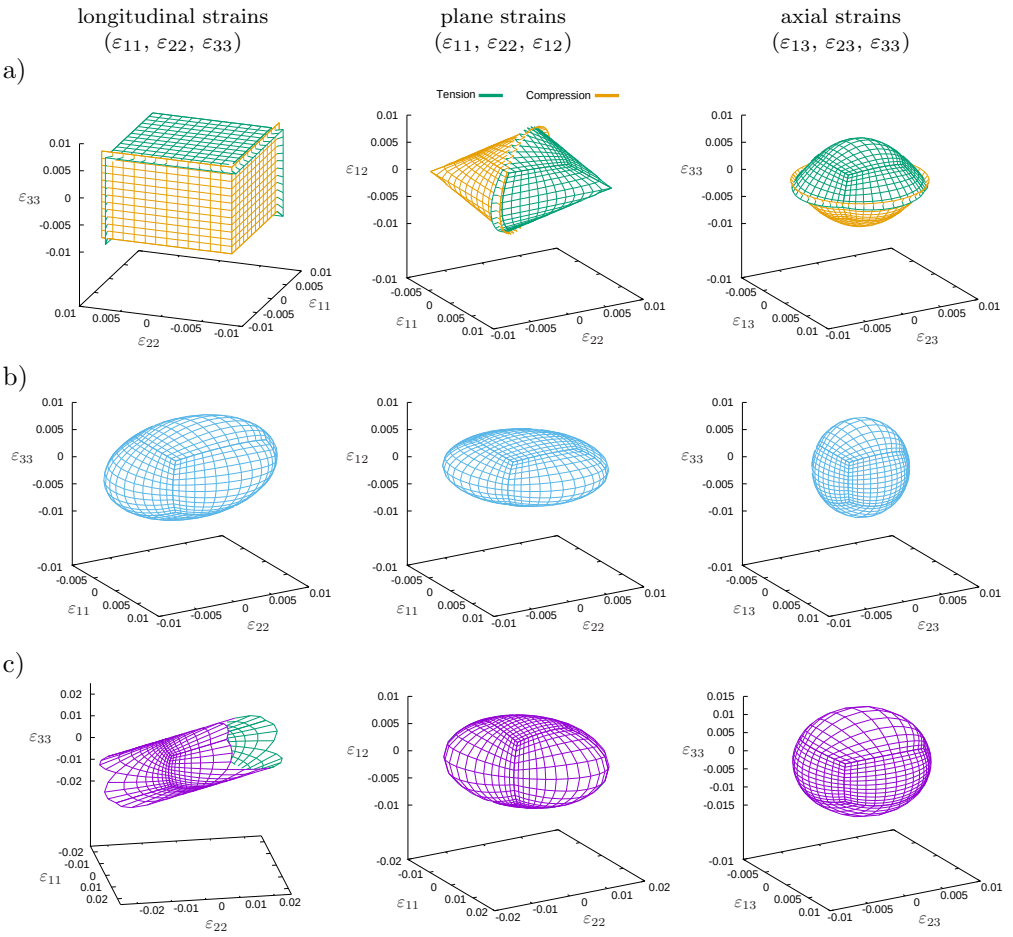

FIG. 3. Damage surfaces corresponding to the local damage criteria: a) max. principal strain ($\epsilon_d^{\mathrm{t}} = 0.0073$, $\epsilon_d^{\mathrm{c}} = 0.0080$), b) energy-based effective strain ($\epsilon_d = 0.007$), c) Huber–von Mises strain ($\epsilon_d = 0.0138$), depicted in three strain component subspaces: longitudinal strains, plane strains, and axial longitudinal/shear strains.

2.4. Global damage criteria

Having defined the local damage criterion, we do also need to define global damage of the cancellous structure at the macro scale. The most restrictive assumption is to consider the entire microstructure damaged when at least one material point (i.e., one Gauss point in the FE model of the microstructure cell)

is damaged at the micro scale, i.e., the local strain-based damage criterion is violated at that point. It seems, however, reasonable to assume that remarkable damage to the structure can only be observed when a certain amount of the material volume is subjected to strains exceeding the damage limit. It is not easy to convincingly define this amount without performing nonlinear analysis of the structure; let us however mention, e.g., [14] where arbitrary values between 1% and 7% of the total material volume were considered. In this work, results are independently presented for the assumed values of 2%, 4% and 6% of the total material volume in the model. This means that damage criterion is allowed to be violated at Gauss points in elements whose total volume constitutes 2%, 4% and 6% of the total FE cell model volume, respectively. Additionally, a set of results denoted by 0% is given for the most restrictive "first blood" assumption mentioned at the beginning of this paragraph.

Remark. Since the analysis was linear, changes in material properties in the domain considered damaged (according to the local damage criterion) were neglected. This simplification is obviously a source of errors as the material at these locations becomes in fact significantly weaker. However, as long as the total volume of damaged material remains small (as it is in this study), it seems justified to consider these errors insignificant.

It is postulated that the macroscopic damage criterion has the form analogous to (2), i.e.,

$$\overline{E} \leq \epsilon_d, \tag{6}$$

where ϵ_d is the damage limit defined in the microscopic criterion and $\overline{E}$ is the value of the macroscopic damage factor determined for a particular macroscopic strain E_{ij} in the above-described numerical experiment. The definition of $\overline{E}$ depends on the choice of the microscopic damage criterion – hence, we consequently distinguish between $\overline{E}^{\mathrm{Pt}}$, $\overline{E}^{\mathrm{Pc}}$, $\overline{E}^{\mathrm{U}}$ and $\overline{E}^{\mathrm{HM}}$ – and the assumed damaged volume limit $n\%$ $(n = 0, 2, 4, 6)$ indicated in the subscript to this symbol. For a particular damage criterion, we define

$$\overline{E}_{n\%} = \max_{P_k \in \mathcal{G} \setminus \mathcal{G}_{n\%}} \overline{\varepsilon}(P_k), \tag{7}$$

where $\mathcal{G}$ is the set of all Gauss integration points P_k in the FE model, and $\mathcal{G}_{n\%}$ is the set of all these integration points at which the local damage factor $\overline{\varepsilon}$ assumes its highest values, while the total FE volume corresponding to those points does not exceed $n\%$ of the total FE model volume. In other words, $\overline{E}_{n\%}$ is the maximum cut-off value of $\overline{\varepsilon}$ in the entire cell model, excluding $n\%$ of its volume where this value is exceeded. Obviously, the set $\mathcal{G}_{0\%}$ is empty and thus $\overline{E}_{0\%}$ is the maximum value of $\overline{\varepsilon}$ in the entire cell.

3. Results

The FE analyses described in the previous sections have been run and their results have been saved in the result files available for download in [11]. For each microstructure instance defined by the geometric parameters t_c, t_h, t_v and for each averaged macroscopic strain state E_{ij} from the considered set of their values, the values of damage factors $\overline{E}$ have been independently computed and saved for the four considered damage criteria and for the four considered damaged volume limits, i.e.,

$$\begin{aligned} &\overline{E}^{\mathrm{Pt}}_{0\%},\ \overline{E}^{\mathrm{Pc}}_{0\%},\ \overline{E}^{\mathrm{U}}_{0\%},\ \overline{E}^{\mathrm{HM}}_{0\%}, \qquad \overline{E}^{\mathrm{Pt}}_{2\%},\ \overline{E}^{\mathrm{Pc}}_{2\%},\ \overline{E}^{\mathrm{U}}_{2\%},\ \overline{E}^{\mathrm{HM}}_{2\%}, \\ &\overline{E}^{\mathrm{Pt}}_{4\%},\ \overline{E}^{\mathrm{Pc}}_{4\%},\ \overline{E}^{\mathrm{U}}_{4\%},\ \overline{E}^{\mathrm{HM}}_{4\%}, \qquad \overline{E}^{\mathrm{Pt}}_{6\%},\ \overline{E}^{\mathrm{Pc}}_{6\%},\ \overline{E}^{\mathrm{U}}_{6\%},\ \overline{E}^{\mathrm{HM}}_{6\%}. \end{aligned} \tag{8}$$

Whenever the damage factor appeared negative (which is possible in the case of the max. principal strain double criterion), zero was written down.

For any of the damage criteria and damaged volume limits, one can compare the resulting value of $\overline{E}$ against the local damage limit value for the corresponding damage criterion to verify whether the assumed macroscopic strain state is safe or not. Since the analysis was linear, one can define the *damage load multiplier* as

$$k_d = \epsilon_d / \overline{E} \tag{9}$$

for the given macroscopic strain state E_{ij} and for the given local damage criterion, such that the scaled strain state $k_d E_{ij}$ belongs to the macroscopic damage surface. This scaled strain state will be further referred to as the *experimental damage point* corresponding to the strain E_{ij} in the 6D space of macroscopic strain components. Obviously, the word "experimental" refers to the numerical experiment here. In the case of $\overline{E} = 0$ the load multiplier k_d is infinite and the experimental damage point does not exist, which means that there is no damage limit in this "direction" of the macroscopic strain load.

All experimental damage points determined for a particular microstructure instance, damage criterion and damaged volume limit, and for all the considered strain states E_{ij}, form a cloud of points in the strain component space. Those points belong to the experimental damage surface for the considered case, thus visualizing its shape. Figure 4 presents examples of such visualization for the microstructure shown in Fig. 2, for different damage criteria and different damaged volume limits.

As mentioned at the end of Sec. 1, our objective is to formulate parameterized equations for damage surfaces in the macroscopic strain space for different damage criteria and damaged volume limits, i.e., equations whose coefficients could be expressed as parametric functions of the microstructure geometric parameters t_c, t_h, t_v. The so expressed damage surfaces should approximate the clouds

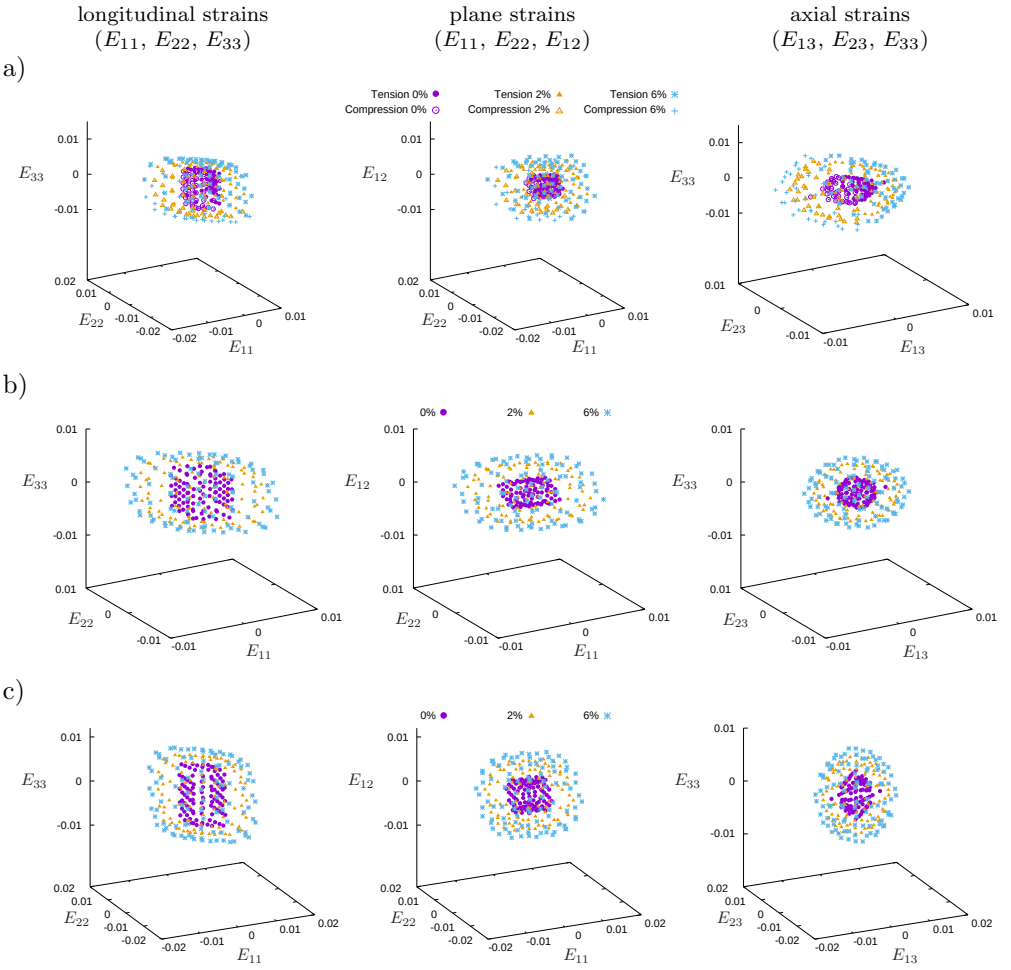

FIG. 4. Experimental damage surfaces given by clouds of points for the microstructure instance defined by $t_c = 0.1$, $t_h = t_v = 0.4$, corresponding to the local damage criteria: a) max. principal strain ($\epsilon_d^{\mathrm{t}} = 0.0073$, $\epsilon_d^{\mathrm{c}} = 0.0104$), b) energy-based effective strain ($\epsilon_d = 0.007$), c) Huber–von Mises strain ($\epsilon_d = 0.0138$), for three levels of allowed damaged volume fraction (0%, 2% and 6%), depicted in three strain component subspaces: longitudinal strains, plane strains, and axial longitudinal/shear strains.

of experimental damage points, such as those shown in Fig. 4. This task appears extremely difficult, as this becomes quite clear after a short glance at this figure. While the local damage surfaces depicted in Fig. 3 have regular shapes that can be easily and accurately expressed by quadric surface equations, no such features can be visible in the macroscopic experimental surfaces in Fig. 4. Especially for low values of damaged volume limit, the points in the corresponding clouds form quite irregular surfaces, which seem rather unlikely to be successfully approximated by either quadric or other smooth analytic (hyper-)surface

equations. Indeed, the author attempted to find the best-fitting quadric surfaces to the resulting experimental point clouds but the approximation errors appeared unacceptably high.

In view of the mentioned difficulties, the parameterized function defining the damage surface at the macro scale will be provided in the form of a numerical procedure rather than a closed-form analytical formula. Let us note that the damage points database, being the result of the computations described above, is based on a regularly spaced mesh of points in the space of microstructure geometric parameters and strain components. Given the values of any data of our interest at the nodes of this mesh, one can quite easily approximate values of the data at any other point in the space by interpolating the known nodal data with the use of – in the simplest case – poly-linear functions defined separately within each hypercube spanned on the mesh nodes. For example, let us consider one of prescribed strains E_{ij} given by Eq. (1). Knowing the computed values of $\overline{E}$ for a particular damage criterion at all "nodal" microstructures considered in the computations, i.e., at t_c, t_h, t_v assuming independently the values from the set:

$$t_{(1)} = 0.05, \quad t_{(2)} = 0.10, \quad t_{(3)} = 0.15, \quad ..., \quad t_{(19)} = 0.95,$$

one can determine the approximate value of $\overline{E}$ for the same strain E_{ij} at a microstructure defined by any other triplet of values t_c, t_h, t_v using the following 3D interpolation. If, e.g.,

$$t_c \in [t_{(i)}, t_{(i+1)}], \qquad t_h \in [t_{(j)}, t_{(j+1)}], \qquad t_v \in [t_{(k)}, t_{(k+1)}],$$

and the dimensionless coordinates within the mesh cube are defined as:

$$\eta_c = \frac{t_c - t_{(i)}}{t_{(i+1)} - t_{(i)}}, \qquad \eta_h = \frac{t_h - t_{(j)}}{t_{(j+1)} - t_{(j)}}, \qquad \eta_v = \frac{t_v - t_{(k)}}{t_{(k+1)} - t_{(k)}},$$

then $\overline{E}(t_c, t_h, t_v)$ is given as:

$$\begin{aligned}
\overline{E}(t_c, t_h, t_v) \approx\ & (1-\eta_c)(1-\eta_h)(1-\eta_v)\,\overline{E}(t_{(i)}, t_{(j)}, t_{(k)}) \\
& + (1-\eta_c)(1-\eta_h)\eta_v\,\overline{E}(t_{(i)}, t_{(j)}, t_{(k+1)}) \\
& + (1-\eta_c)\eta_h(1-\eta_v)\,\overline{E}(t_{(i)}, t_{(j+1)}, t_{(k)}) \\
& + (1-\eta_c)\eta_h\eta_v\,\overline{E}(t_{(i)}, t_{(j+1)}, t_{(k+1)}) \\
& + \eta_c(1-\eta_h)(1-\eta_v)\,\overline{E}(t_{(i+1)}, t_{(j)}, t_{(k)}) \\
& + \eta_c(1-\eta_h)\eta_v\,\overline{E}(t_{(i+1)}, t_{(j)}, t_{(k+1)}) \\
& + \eta_c\eta_h(1-\eta_v)\,\overline{E}(t_{(i+1)}, t_{(j+1)}, t_{(k)}) \\
& + \eta_c\eta_h\eta_v\,\overline{E}(t_{(i+1)}, t_{(j+1)}, t_{(k+1)}).
\end{aligned} \tag{10}$$

Further, in order to find $\overline{E}(t_c, t_h, t_v, E_{11}, E_{22}, E_{33}, E_{23}, E_{31}, E_{12})$ corresponding to an arbitrary strain E_{ij} not included in the mesh defined by Eq. (1), the interpolation scheme (10) must be extended to the higher-dimensional space in which the strain components defined in Eq. (1) constitute an additional hyper-cubic mesh on whose nodes the extended poly-linear interpolation functions must also be spanned (here the formula is slightly more complicated as the strain E_{ij} must be first scaled so that the highest component value equals ± 0.001, after which Eq. (10) is applied in its extended $(3+5)$D form, with the highest strain component fixed).

An easy-to-use Fortran subroutine implementing the above interpolation scheme is provided along with the data available in [11]. Given the values of the geometric parameters t_c, t_h, t_v and the macroscopic strain components E_{ij} as input, the subroutine returns a table of macroscopic damage factor values (8). Substituting any of these values to Eq. (9), with the damage limit ϵ_d specific to the corresponding damage criterion, one obtains the scale factor that allows to find the damage surface point $k_d E_{ij}$, which is related to the input strain E_{ij} and to the damage criterion considered. Hence, the above scheme and subroutine may be used as a numerical tool to determine the damage surfaces in the strain component space, corresponding to the local damage criteria (2)–(5), as functions of the microstructure geometric parameters.

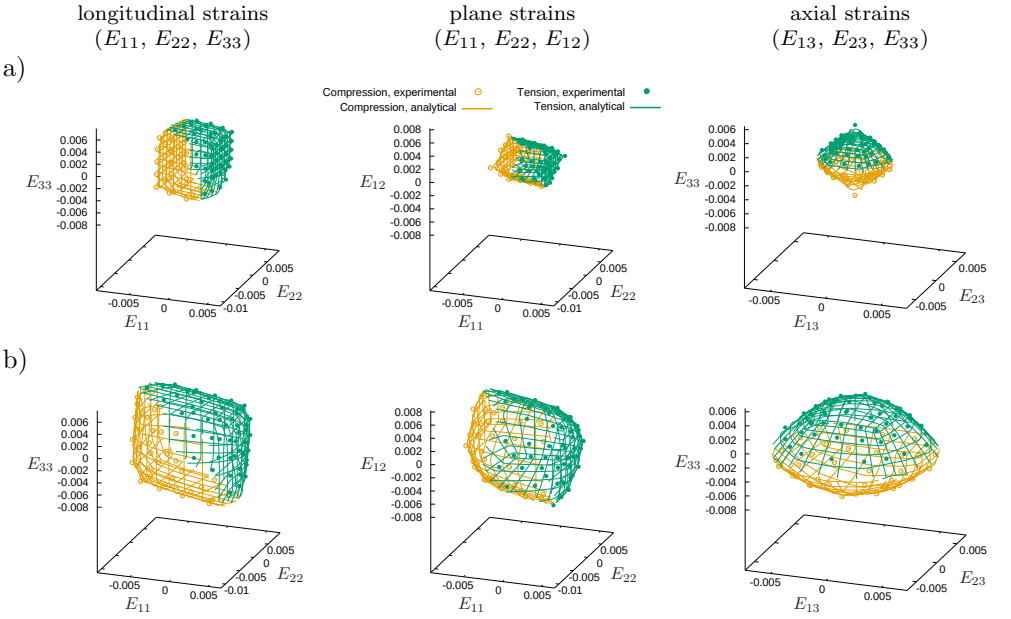

FIG. 5. Analytical interpolated damage surfaces for the microstructure instance defined by $t_c = 0.1$, $t_h = t_v = 0.4$, corresponding to the max. principal strain local damage criterion for a) 0% and b) 2% allowed damaged volume fraction, depicted in three strain component subspaces: longitudinal strains, plane strains, and axial longitudinal/shear strains.

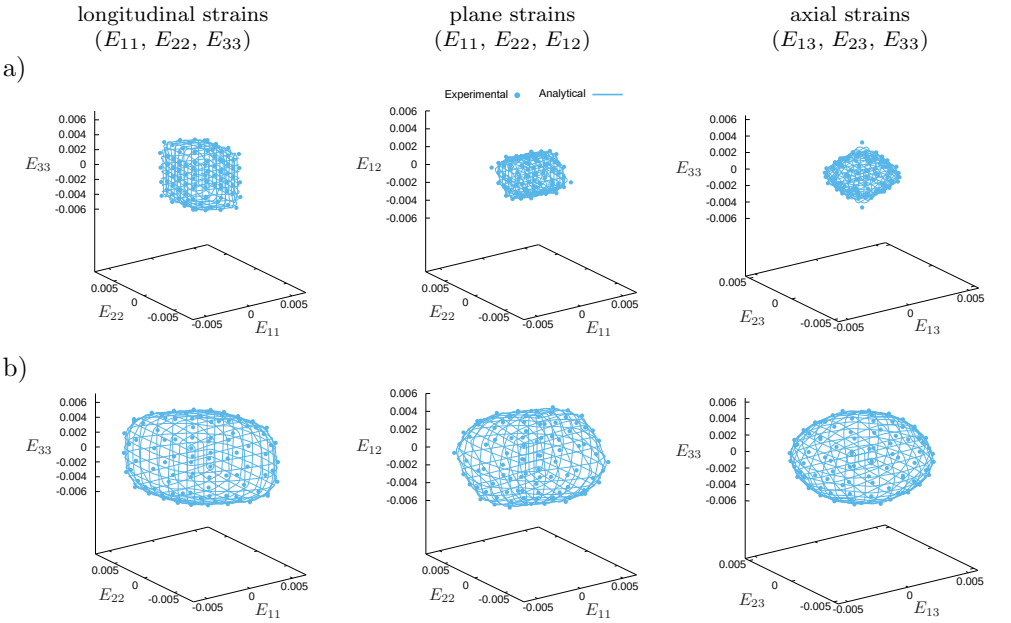

FIG. 6. Analytical interpolated damage surfaces for the microstructure instance defined by $t_c = 0.1$, $t_h = t_v = 0.4$, corresponding to the strain energy-based local damage criterion for a) 0% and b) 2% allowed damaged volume fraction, depicted in three strain component subspaces: longitudinal strains, plane strains, and axial longitudinal/shear strains.

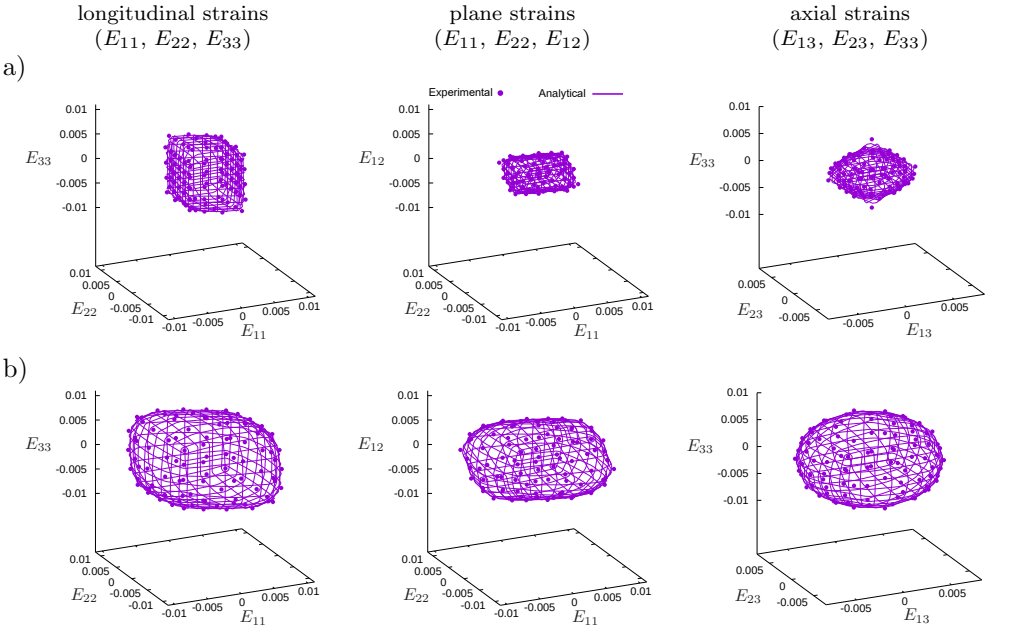

FIG. 7. Analytical interpolated damage surfaces for the microstructure instance defined by $t_c = 0.1$, $t_h = t_v = 0.4$, corresponding to the Huber–von Mises local damage criterion for a) 0% and b) 2% allowed damaged volume fraction, depicted in three strain component subspaces: longitudinal strains, plane strains, and axial longitudinal/shear strains.

Figures 5–7 show examples of analytical damage surfaces in the macroscopic strain component space, determined with the scheme described above. These surfaces are all drawn for the microstructure presented in Fig. 2 and for selected damage criteria, damaged volume limits and 3D subspaces of the strain component space.

4. Discussion

The main output of the presented research is the complete database of macroscopic damage properties of parameterized cellular microstructures mimetizing cancellous bone. The results of the numerical experiments consisting of FE analyses of microstructure cells are available for download from the open data repository, see [11]. This data allow to explicitly determine damage limit values for prescribed microstructure geometries, damage criteria and macroscopic strain-driven loads.

As it can be seen in Fig. 4, the damage surfaces, visualized in the strain component space as clouds of damage points determined in the above-described way, assume quite regular shapes. These surfaces constitute a basis to formulate an extended approach to determine damage points for any possible microstructure geometry and for any macroscopic strain, other than those considered in the analyses. In this study, a poly-linear interpolation scheme is proposed for this purpose. Realizing that both the set of microstructure geometric parameters and the set of strain loads considered in the reported analyses form a regular mesh in their value ranges, one can find the interpolation of the results within the entire domains of the parameter values an easy and straightforward task. As mentioned in the previous Sec. 3, among the data deposited in [11], one can find the source of an easy-to-use Fortran subroutine that performs this interpolation. The proposed numerical procedure may serve as a numerical implementation of the parametric damage surface equation for the considered family of bone-like microstructures. The so defined damage surface is exact at the mesh points obtained from the numerical experiments and approximate elsewhere.

There are other possible ways to determine the damage surface equation in the space of strain components and the microstructure geometric parameters. One of them is to formulate an analytical hyper-surface equation in the space of strain components, with the equation coefficients being functions of the geometric parameters. As mentioned in the previous section, attempts to determine such an equation in the most natural 6D quadric form did not appear satisfactory, as the approximation errors with respect to the experimental data were unacceptably high.

Another possible approach to this problem is to employ neural networks or other machine learning methods. Having trained the network on the data base

of numerical experiment results, one may prepare an AI-driven procedure for predicting damage conditions in an arbitrary case of microstructure geometry and macroscopic strain. The author believes that the results of this research provide a good basis for investigating this promising research area.

Practical application of the presented methods and results in the damage analysis of real bones may raise questions on: (i) which of the local damage criteria (3)–(5) to choose and (ii) how to relate the equivalent microstructure parameters t_c, t_h, t_v to the particular geometry of a given real bone microstructure. Regarding the first issue, it is presumed that mechanical properties of the trabecular tissue constituting the analysed bone are known to the user. In practice, this may pose a problem, as tissue damage data are usually not easily available and one must frequently rely on literature reports and own estimations of analogies between the bone for which the data are available and the one under analysis. The damage models used in this study were reported and tested for different types of bone obtained from various species and locations. The maximum principal strain was reported as the damage factor in [2] (human femoral neck), [5] (sheep vertebrae) and [13] (bovine tibia). The energy-based effective strain was considered the damage factor in [14] (human radius) while the Huber–von Mises theory was applied in [7, 8] (human femur). In all the above studies, values for the local damage limits were also reported. Besides, the three damage criteria were employed and compared in the damage analysis of human femur samples in [15], with the conclusion indicating the maximum principal strain criterion to be the best estimation of reality. These reports, although very selective, may serve as hints for selecting the appropriate local damage model in a particular case analysed.

Regarding the second issue, let us recall a number of standard morphometric parameters (e.g., BV/TV, MIL, VO, SLD) that are usually determined for micro-CT scans of real cancellous bones and are commonly used to quantitatively characterize their microstructure geometry. They may also be computed for equivalent microstructures [10], and thus related to the geometric parameters defining the microstructures. The extensive, publicly available database associated with [10] may be employed to select the equivalent microstructure geometry that fits best (in terms of morphometric parameter values) the real bone microstructure under consideration.

Resuming, this study is – to the author's best knowledge – the first systematic approach to the macroscopic damage analysis of cancellous bone and bone-like cellular materials. The extensive database of damage results provided here constitutes the basis to predict damage conditions in a variety of cancellous microstructures in a general, parametric manner. Additionally, it enables search for efficient numerical methods that make this prediction as automated and accurate as possible. It is noteworthy that these results may be not only

applicable in numerical biomechanics but also in structural engineering, design and optimization, where the use of biomimetic materials is gaining increasing interest. The data provided in this study may be used in the numerical design, analysis and optimization of such materials and of structures made from them.

References

1. H.H. Bayraktar, A. Gupta, R.Y. Kwon, P. Papadopoulos, T.M. Keaveny, The modified super-ellipsoid yield criterion for human trabecular bone, *Transactions of ASME, Journal of Biomechanical Engineering*, **126**: 677–684, 2004, https://doi.org/10.1115/1.1763177.
2. H.H. Bayraktar, E.F. Morgan, G.L. Niebur, G.E. Morris, E.K. Wong, T.M. Keaveny, Comparison of the elastic and yield properties of human femoral trabecular and cortical bone tissue, *Journal of Biomechanics*, **37**: 27–35, 2004, https://doi.org/10.1016/S0021-9290(03)00257-4.
3. L. Colabella, A.P. Cisilino, G. Häiat, P. Kowalczyk, Mimetization of the elastic properties of cancellous bone via a parameterized cellular material, *Biomechanics and Modeling in Mechanobiology*, **16**: 1485–1502, 2017, https://doi.org/10.1007/s10237-017-0901-y.
4. M. Frank, A.G. Reisinger, D.H. Pahr, P.J. Thurner, Effects of osteoporosis on bone morphometry and material properties of individual human trabeculae in the femoral head, *JBMR Plus*, **5**(6): e10503, 2021, https://doi.org/10.1002/jbm4.10503.
5. N.M. Harrison, P. McDonnell, L. Mullins, N. Wilson, D. O'Mahoney, P.E. McHugh, Failure modelling of trabecular bone using a non-linear combined damage and fracture voxel finite element approach, *Biomechanics and Modeling in Mechanobiology*, **12**: 225–241, 2013, https://doi.org/10.1007/s10237-012-0394-7.
6. J. Kabel, B. van Rietbergen, M. Dalstra, A. Odgaard, R. Huiskes, The role of an effective isotropic tissue modulus in the elastic properties of cancellous bone, *Journal of Biomechanics*, **32**(7): 673–680, 1999, https://doi.org/10.1016/S0021-9290(99)00045-7.
7. J.H. Keyak, S.A. Rossi, Prediction of femoral fracture load using finite element models: An examination of stress- and strain-based failure theories, *Journal of Biomechanics*, **33**(2): 209–214, 2000, https://doi.org/10.1016/S0021-9290(99)00152-9.
8. J.H. Keyak, Improved prediction of proximal femoral fracture load using nonlinear finite element models, *Medical Engineering and Physics*, **23**(3): 165–173, 2001, https://doi.org/10.1016/S1350-4533(01)00045-5.
9. P. Kowalczyk, Elastic properties of cancellous bone derived from finite element models of parameterized microstructure cells, *Journal of Biomechanics*, **36**(7): 961–972, 2003, https://doi.org/10.1016/S0021-9290(03)00065-4.
10. P. Kowalczyk, Orthotropic properties of cancellous bone modelled as parameterized cellular material, *Computer Methods in Biomechanics and Biomedical Engineering*, **9**(3): 135–147, 2006, https://doi.org/10.1080/10255840600751473.
11. P. Kowalczyk, Parametric damage data of cellular bone-like microstructures, RepOD, 2025, https://doi.org/10.18150/4SOSUD.
12. R.K. Nalla, J.H. Kinney, R.O. Ritchie, Mechanistic fracture criteria for the failure of human cortical bone, *Nature Materials*, **2**: 164–168, 2003, https://doi.org/10.1038/nmat832.

13. G. Niebur, M.J. Feldstein, J.C. Yuen, T.J. Chen, T.M. Keaveny, High-resolution finite element models with tissue strength asymmetry accurately predict failure of trabecular bone, *Journal of Biomechanics*, **33**: 1575–1583, 2000, https://doi.org/10.1016/S0021-9290(00)00149-4.

14. W. Pistoia, B. van Rietbergen, E.-M. Lochmüller, C.A. Hill, P. Rüegsegger, Estimation of distal radius failure load with micro-finite element analysis models based on three-dimensional peripheral quantitative computed tomography images, *Bone*, **30**(6): 842–848, 2002, https://doi.org/10.1016/s8756-3282(02)00736-6.

15. E. Schileo, F. Taddei, L. Cristofolini, M. Viceconti, Subject-specific finite element models implementing a maximum principal strain criterion are able to estimate failure risk and fracture location on human femurs tested in vitro, *Journal of Biomechanics*, **41**: 356–367, 2008, https://doi.org/10.1016/j.jbiomech.2007.09.009.

16. B. van Rietbergen, H. Weinans, R. Huiskes, A. Odgaard, A new method to determine trabecular bone elastic properties and loading using micromechanical finite-element models, *Journal of Biomechanics*, **28**(1): 69–81, 1995, https://doi.org/10.1016/0021-9290(95)80008-5.

Received June 18, 2025; revised version September 18, 2025; accepted September 19, 2025; published online September 30, 2025.